# Numerical investigation of dynamic stall on wings following curved trajectory

Yu-Cheng Lu<sup>1</sup>, Vitor G. Kleine<sup>2</sup>, Ardeshir Hanifi<sup>1</sup>, and Dan S. Henningson<sup>1</sup>

<sup>1</sup>FLOW, Department of Engineering Mechanics, KTH Royal Institute of Technology, Stockholm, Sweden
E-mail:, ycl@kth.se, hanifi@kth.se, henning@mech.kth.se

<sup>2</sup>Division of Aeronautic Engineering, Instituto Tecnológico de Aeronáutica, São José dos Campos, Brasil
E-mail:, kleine@ita.br

# **Abstract**

Unsteady aerodynamic flows play a pivotal role in both engineering applications and natural phenomena, with dynamic stall representing a particularly critical challenge. This phenomenon not only degrades aerodynamic efficiency but also induces unsteady loads and aeroelastic responses that can compromise structural integrity. However, the evolution of dynamic stall under complex kinematics remains inadequately understood. This study aims to advance the understanding of dynamic stall mechanisms and to develop computationally efficient models that retain essential nonlinear flow features. We first employ high-fidelity direct numerical simulations (DNS) using the spectral element solver Nek5000 to study a wing undergoing circular motion at the reduced frequencies k = 0.6, representing light stall conditions. Modal analysis, such as proper orthogonal decomposition, was applied to the spanwise vorticity field to better understand the evolution of the dynamic stall vortex and the corresponding flow structures. Despite the accuracy of DNS, its high computational cost limits its practical application and the feasibility to study the far wake. Thus, the second part of this study explores a reduced-order modelling approach using an advanced actuator line model to investigate dynamic stall on a plunging wing. While conventional actuator line models have inherent limitations in capturing unsteady phenomena, we incorporate force coefficients extracted from DNS results to reconstruct the flow fields within the actuator line model to bridge this gap. The spectrum of the induced velocity is compared with analytical results from a novel linear theory for unsteady aerodynamics in actuator line method (Alva et al. 2025). The results demonstrate that the advanced actuator line method is capable of capturing parts of the unsteady effect from dynamic stall and the near wake. This highlights the potential to model dynamic stall using the actuator line method and underscores the feasibility of integrating a dynamic stall model and wake study within this approach.

**Keywords:** Unsteady aerodynamics, Dynamic stall, Direct numerical simulation, Actuator line method

## 1 Introduction

Unsteady aerodynamic flows play a crucial role in numerous engineering applications and aspects of everyday life. In aeronautical engineering, unsteady aerodynamics affects not only lift and drag but also aircraft stability, fuel efficiency, and noise emissions. In the context of renewable energy, particularly wind power, power output and structural longevity are closely tied to the behavior of unsteady aerodynamic flows. Among various unsteady aerodynamic phenomena, dynamic stall is particularly critical, as it degrades aerodynamic performance and induces aeroelastic responses that can lead to

structural fatigue.

Dynamic stall occurs when an airfoil undergoes unsteady motion, such as pitching, and exceeds its static stall angle. This results in a large transient overshoot in aerodynamic forces due to boundary layer separation and the subsequent formation of a dynamic stall vortex near the leading edge. Dynamic stall is a key consideration in aircraft maneuvering [1], rotor and wind turbine performance [2], and the flight of birds and insects [3, 4]. Therefore, understanding and controlling unsteady aerodynamic flow and dynamic stall is essential for improving aerodynamic efficiency and enabling sustainable aviation through drag reduction and improved energy perform-

ance.

Significant research has been conducted to understand dynamic stall mechanisms, primarily through studies of oscillating pitching [5] and plunging wings [6, 7]. These investigations often rely on high-fidelity simulations that provide detailed flow structures; however, such methods are computationally intensive and less practical for engineering applications. It is also difficult to resolve the far wake due to the computational cost. Moreover, real-world scenarios such as aircraft maneuvers involve complex trajectories where additional effects, like Coriolis forces, come into play and influence the onset and development of dynamic stall [8].

To address the challenge regarding computational cost and far wake modeling, various alternative simulation techniques have been developed. One notable example is the Actuator Line Method (ALM), developed and widely used in wind energy applications [9, 10]. It is also utilised to the simulation of fixed-wing airplane [11]. The actuator line method offers several advantages, including computational efficiency, the ability to capture three-dimensional effects at lower cost, and the capability to simulate wakes. In ALM, the wing geometry is represented as a line of distributed forces, and aerodynamic forces are typically estimated using thin airfoil theory. However, this conventional approach struggles to capture unsteady effects like dynamic stall accurately. Recent advancements have extended ALM using linear unsteady aerodynamic theories, enabling modeling of plunging wing motions at low reduced frequencies [12]. These developments highlight the need for further research into unsteady flow phenomena involving complex motion and the enhancement of ALM for such applications.

To explore dynamic stall in a representative unsteady flow scenario and evaluate the capability of ALM in capturing such effects, we focus on a case inspired by vertical-axis wind turbines (VAWTs), where the wing moves in a periodic circular trajectory (see Figure 1). This type of motion has been widely studied due to its relevance to dynamic stall and its relative simplicity compared to full aircraft maneuvers. Experimental investigations employing particle image velocimetry (PIV) have revealed detailed vortex dynamics in such setups [2, 13]. Numerical approaches such as Unsteady Reynolds-Averaged Navier-Stokes (URANS) and Large Eddy Simulations (LES) often using rotating meshes [14, 15] or simplify the motion by modulating inflow conditions [16]. More recently, Direct Numerical Simulations (DNS) have been conducted and analyzed using Proper Orthogonal Decomposition (POD) to study dynamic stall under varying rotational speeds [17]. On the other hand, the success of ALM in unsteady aerodynamic effects indicates the potential of applying ALM simulations to model the unsteady flow phenomena such as dynamic stall. This study aims to provide deeper insights into the chosen flow case using high-fidelity DNS, alongside evaluating the performance and characteristics of ALM in capturing unsteady flow features. The ultimate goal is to inform the development of the novel actuator line method that balances computational efficiency and accuracy for dynamic stall modelling, which can further facilitate the far wake investigation of the unsteady aerodynamic flows with dynamic stall, together with the sophisticated results from DNS.

In the present work, we investigate the flow around a wing undergoing circular motion using both DNS and ALM. Section 2 introduces the wing kinematics, and Section 3 details the numerical methodologies. The results and discussion are presented in Section 4, followed by conclusions in Section 5.

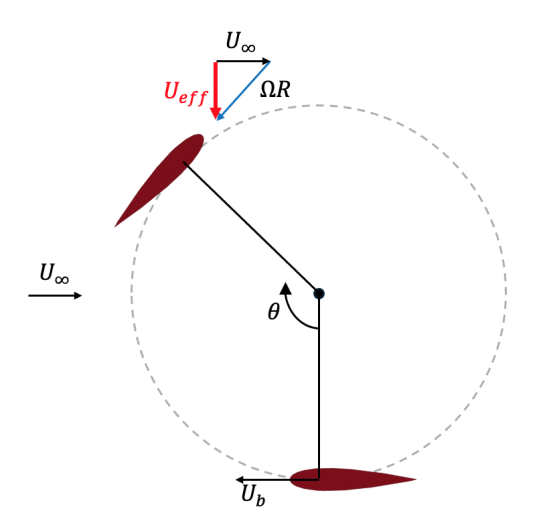


Figure 1: Illustration of the wing kinematics

### 2 Case of Study

This study investigates the unsteady flow around a NACA 0018 airfoil undergoing periodic circular motion. The simulations are conducted at a chord-based Reynolds number of  $Re_c = \Omega Rc/v = 50,000$ , where  $\Omega$  is the angular velocity, R is the rotational radius, c is the chord length, and v is the kinematic viscosity of the fluid. The wing follows a circular trajectory with a radius of 2.5c, and the motion corresponds to a reduced frequency of  $k = \Omega b/U_\infty = 0.6$ , where b = c/2 and  $U_\infty$  is the free-stream velocity. Figure 2 shows the geometric effective angle of attack  $\alpha_{eff,g}$ , calculated using Equation 1. During each cycle, the airfoil exceeds the static stall angle  $\alpha_{ss}$  twice: first at t = 0.17T during the upwind pass, and again at t = 0.59T, indicating the periodic occurrence of dynamic stall. The detailed numerical methods and simulation setup for this case are presented in Section 3.

$$\alpha_{eff,g}(\theta) = tan^{-1} \left( \frac{\sin \theta}{2kR + \cos \theta} \right),$$
 (1)

# 3 Methods

### 3.1 Direct numerical simulation

The direct numerical simulations (DNS) in this study were conducted using the open-source, high-order spectral element method (SEM) code Nek5000 [18]. The velocity and pressure fields are represented using Lagrange polynomial expansions on Gauss–Lobatto–Legendre (GLL) and Gauss–Legendre (GL) quadrature points, respectively. Spatial discretization follows the  $\mathbb{P}_N - \mathbb{P}_{N-2}$  formulation for solving the unsteady,

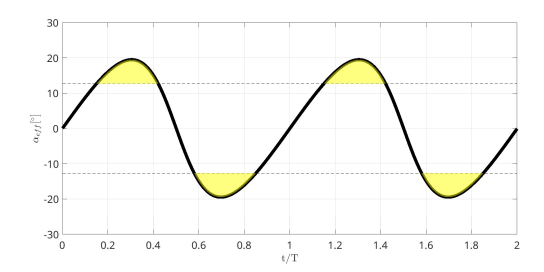


Figure 2: Geometric effective angle of attack  $\alpha_g$ . The yellow shaded area is the time period when the wing exceeds the static stall angle.

three-dimensional incompressible Navier–Stokes equations. Time integration is performed using a third-order backward differentiation formula (BDF3) for the diffusive terms and a third-order extrapolation (EXT3) scheme for the nonlinear terms. To meet DNS resolution requirements, the computational mesh is refined to maintain wall-unit spacing  $\Delta y^+ < 0.4$ ,  $\Delta x^+ < 20$ , and  $\Delta z^+ < 10$ .

The NACA0018 wing has a span of 0.2c with the periodic boundary condition at the spanwise direction. To incorporate the movement of the wing, we implement the overlapping overset grid NekNek [19] framework with two computational domains in the simulation. The inner domain controls the wing movement by rotating at a constant angular velocity according to the reduced frequency. It includes the wing and the surrounding flow field with radius 5.0c. The static outer domain serves as the far field of the computational domain with the size of 40c at each boundary. The interface between the two domains is treated with a Dirichlet boundary condition, updated at every time step through interpolation. Figure 3 illustrates the DNS domain configuration. The inlet is applied with the Dirichlet boundary condition, and the stabilised outflow boundary condition [20] is set for the outlet.

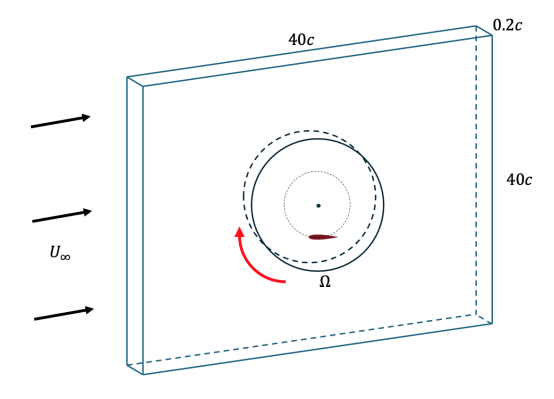


Figure 3: Computational domain of DNS.

The initial condition of the flow field was obtained by using ANSYS Fluent® v23.1 to perform the two-dimensional unsteady Reynolds-averaged Navier-Stokes (URANS) simulation with SST  $k-\omega$  turbulence model [21]. After initializing the DNS for two full motion periods, flow field snapshots and aerodynamic force data were collected over eight additional cycles. Each cycle includes 200 flow snapshots, and aerody-

namic forces were sampled at a frequency of 1200 points per period.

### 3.2 Proper orthogonal decomposition

The features of the unsteady flow phenomenon and turbulent coherent structures can be extracted by the modal analysis technique, such as proper orthogonal decomposition (POD) [22]. POD provides the spatial modes  $\phi_n(x,y,z)$  and the corresponding time coefficients  $a_n(t)$  from the decomposition of the 1600 snapshots from eight rotational periods as expressed in Equation 2. The POD analysis on the three-dimensional spanwise vorticity  $(\omega_z)$  field from DNS was performed in the present study, facilitating the understanding to the formation and evolution of coherent structures, particularly those associated with the onset of dynamic stall.

$$\omega_z(x, y, z, t) = \sum_{n=1}^{N} a_n(t)\phi_n(x, y, z)$$
 (2)

#### 3.3 Actuator line model simulation

The actuator line method (ALM) simulations were conducted using the open-source spectral code Dedalus [23]. The computational domain, defined in a Cartesian coordinate system, comprises a Fourier spectral grid with  $[N_x, N_y] = [256, 128]$  points in the streamwise and normal directions, respectively.

In the ALM simulations, aerodynamic forces are distributed throughout the domain by smoothing them around the actuator line with a Gaussian kernel. The smoothing width is defined by  $\varepsilon/c=0.4$ , 0.8, and 1.6, where the chord length c=1.0. Although ALM conventionally calculates forces using thin-airfoil theory, the present simulations incorporate lift and drag forces as the two-dimensional body force per spanwise unit length

$$\mathbf{F}_{2D} = (L_{ALM}, D_{ALM}) = \left(\frac{1}{2}\rho u_r cC_l, \frac{1}{2}\rho u_r cC_d\right), \quad (3)$$

where  $u_r$  is the relative velocity, sampled at the actuator point. The lift and drag coefficients are directly extracted from the DNS results and scaled by the geometric effective velocity

$$U_{eff}(\theta) = U_{\infty} \sqrt{1 + 2kR\cos\theta + (2kR)^2},$$
 (4)

as defined in Equations 5 and 6, to properly impose the unsteady aerodynamic effects, including dynamic stall, within the ALM simulations.

$$C_l = \frac{L_{DNS}}{0.5\rho U_{eff}^2 sc} \tag{5}$$

$$C_d = \frac{D_{DNS}}{0.5\rho U_{eff}^2 sc} \tag{6}$$

The two-dimensional body force  $\mathbf{F}_{2D}$  is then distributed in the computational domain by the Gaussian kernel as expressed in Equation 7.

$$\mathbf{f} = -\mathbf{F}_{2D} \frac{1}{\varepsilon^2 \pi} exp\left(-\frac{x^2 + y^2}{\varepsilon^2}\right) \tag{7}$$

Unlike the DNS setup, the actuator line in ALM remains stationary. This simplification isolates the modeling capability of ALM for unsteady aerodynamic phenomena, particularly dynamic stall. Similar stationary setups, where only the pitching condition is varied without physical wing motion, have been previously employed in URANS and Detached Eddy Simulations (DES), and validated against experimental data [16].

In addition to the ALM simulations, we apply the linear-theory-based unsteady aerodynamic model proposed in [12] to compute the induced velocity at the actuator line for comparison. The vertical induced velocity  $u_y$  is obtained from Equation 8, where  $\hat{u}_y$  is the Fourier transform of the vertical velocity,  $\kappa$  is a complex function of  $\varepsilon/c$  as introduced in [12], and  $\hat{\Gamma}$  is the Fourier transform of circulation, which is computed using Equation 9.

$$\hat{u}_{y}(0,0,0) = \kappa(k_{\varepsilon})\hat{\Gamma} \tag{8}$$

$$\Gamma = \frac{U_{\infty}cC_l}{2} \tag{9}$$

Once the induced velocity at the actuator line is known, the effective angle of attack  $\alpha_{eff}$  can be evaluated. In the conventional ALM, the effective angle of attack

$$\alpha_{eff,ALM} = \alpha_{eff,g} + tan^{-1} \left(\frac{u_y}{u_x}\right)$$
 (10)

accounts for both the geometric angle of attack  $\alpha_{eff,g}$  and induced velocities, as shown in Equation 10. For the linear-theory-based model, the streamwise velocity  $u_x$  is taken as the freestream value  $U_{\infty}=1.0$ , and the vertical velocity  $u_y$  is computed from Equation 8. To incorporate unsteady effects more accurately, the model is modified by adding a term proportional to the pitching rate  $\dot{\alpha}_{eff,g}$ , as suggested in [12], and expressed in Equation 11, where the coefficient a=-1/2.

$$\alpha_{eff,m} = \alpha_{eff,g} + tan^{-1} \left(\frac{u_y}{u_x}\right) + b\left(\frac{1}{2} - a\right) \dot{\alpha}_{eff,g} \quad (11)$$

### 4 Results

# 4.1 Direct numerical simulation

The direct numerical simulation (DNS) captures the detailed evolution of the dynamic stall vortex and the near-wake flow structures. Figures 4 and 5 present snapshots of the flow field and spanwise vorticity, respectively. As the wing moves through the upwind region, a dynamic stall vortex gradually develops on the suction side. At t = 0.35T, this vortex begins to separate from the wing surface. Simultaneously, a trailing edge vortex starts to form and roll up. By t = 0.5T, the dynamic stall vortex has fully detached from the suction side, coinciding with a significant growth of the trailing edge vortex. Before the wing exceeds the static stall angle  $\alpha_{ss}$  again in the downwind region (t = 0.55T), both the dynamic stall vortex and the trailing edge vortex have separated completely. At

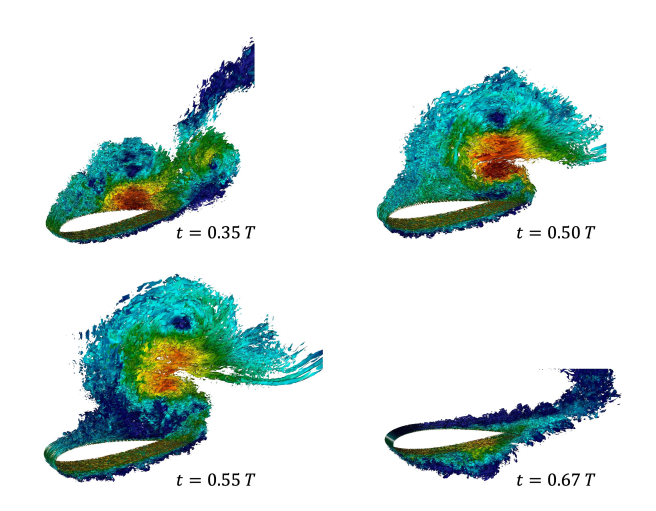


Figure 4: Snapshots of  $\lambda_2$  structure colored by velocity magnitude

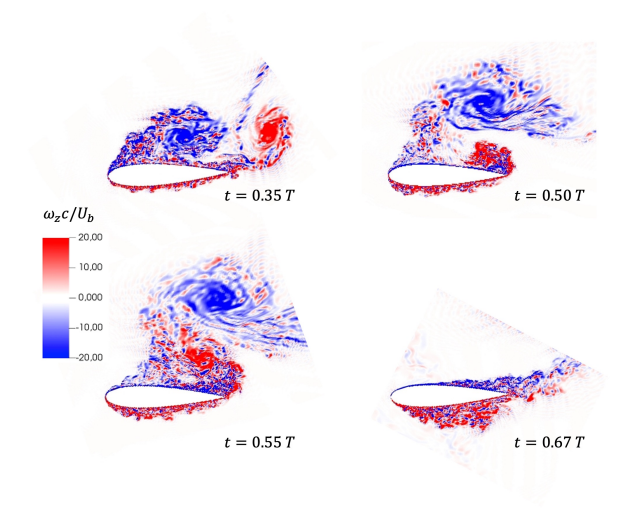


Figure 5: Spanwise vorticity ( $\omega_z$ ) field at z = 0.1

t = 0.67T, although turbulent structures appear on the suction side, a new dynamic stall vortex does not form.

The phase-averaged lift and drag coefficients are shown in Figure 6. The lift coefficient  $C_l$  increases with the growth of the dynamic stall vortex and peaks at  $C_l = 2.14$  at t = 0.35T. At this time, the drag coefficient  $C_d$  reaches its minimum value of -0.52. Following the lift stall,  $C_l$  decreases to a minimum of -0.57 at t = 0.67T, before gradually rising again with minor fluctuations. In contrast,  $C_d$  increases from t = 0.35T, peaking at  $C_d = 0.5$  at t = 0.49T, then decreases to a local minimum of -0.09 at t = 0.67T, remaining within a similar range during the downwind region. Figure 7 presents the time evolution of the pitching moment coefficient  $C_{mp}$ . The growth of the dynamic stall vortex induces a negative pitching moment, with  $C_{mp}$  reaching a minimum of -0.21 at the same instant that  $C_l$  peaks and  $C_d$  is minimized. The maximum value of the pitching moment coefficient  $C_{mp} = 0.02$ occurs at t = 0.67T, corresponding to the minimum lift. These variations in lift and pitching moment induced by dynamic stall are critical factors contributing to aeroelastic fatigue. A comparison with the geometric effective angle of attack  $\alpha_{eff,g}$  reveals a delay of approximately 0.2T between the dynamic lift stall and the moment the wing exceeds the static stall angle. Notably, dynamic stall occurs periodically only in the upwind region, despite the wing also exceeding  $\alpha_{ss}$  on the downwind side.

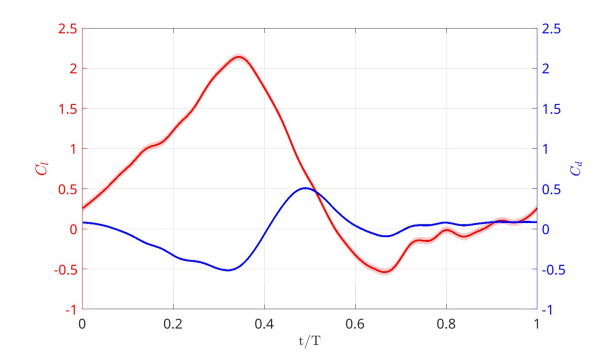


Figure 6: Phase-averaged lift and drag coefficient plot.

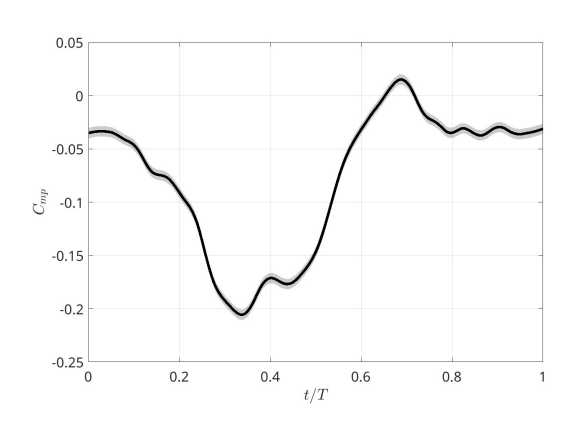


Figure 7: Phase-averaged pitching moment coefficient plot.

To investigate the dominant flow structures throughout the rotation, proper orthogonal decomposition (POD) is applied to the spanwise vorticity field. The second and third POD modes reflect the development of the dynamic stall vortex, as indicated by the increasing negative magnitude of their time coefficients during the upwind phase (see Figure 8). The third mode also captures the formation of the trailing edge vortex. Figure 9 illustrates the onset of vortex separation, marked by the detachment of the dynamic stall vortex and the simultaneous roll-up of the trailing edge vortex.

## 4.2 Actuator line method

Actuator line method (ALM) simulations were conducted using three different Gaussian width parameters  $\varepsilon/c=0.4,0.8$ , and 1.6 within the *Dedalus* simulations. In these simulations, the lift and drag forces from eight DNS periods were imposed on the actuator line. As  $\varepsilon/c$  increases, the aerodynamic forces are distributed over a wider area in the computational domain. To assess the effect of  $\varepsilon/c$  and validate the accuracy of the linear theory approximation, the vertical induced velocity at the actuator line  $u_y(0,0,0)$  was extracted from the ALM simulations and compared to theoretical predictions from Equa-

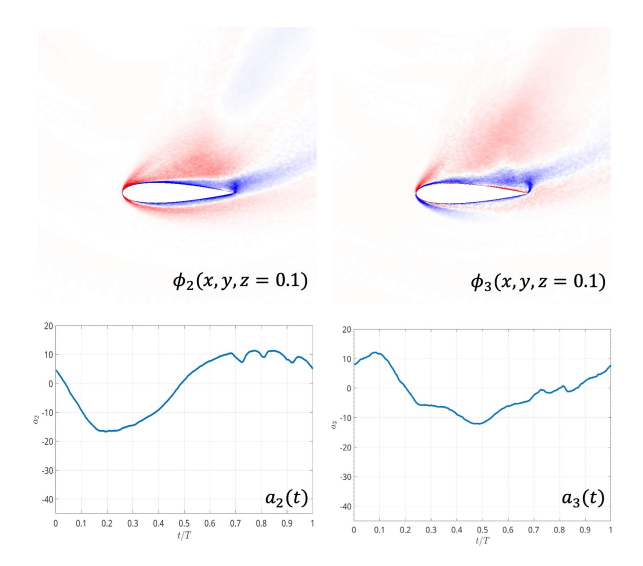


Figure 8: Second and third spatial modes and corresponding time coefficients

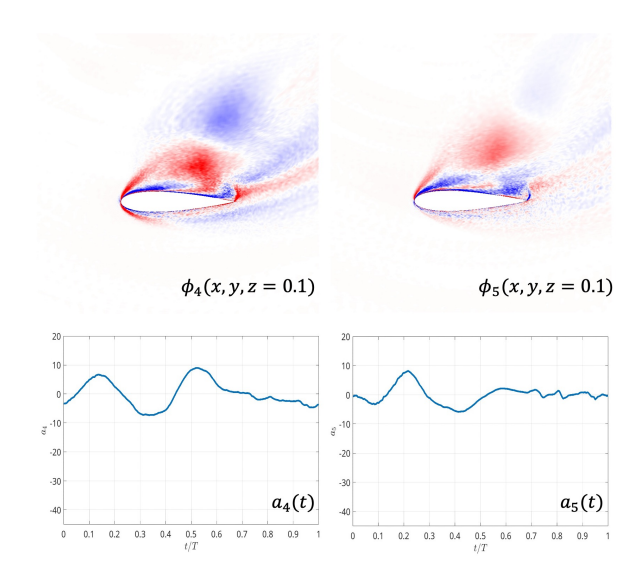


Figure 9: Forth and fifth sptial modes and corresponding time coefficients

tion 8. The magnitude spectra of the induced velocity are shown in Figure 10, demonstrating good agreement between the ALM simulations and the linear theory. Table 1 presents the ratio between the linear theory and ALM simulation results ( $\hat{v}_{Linear}/\hat{v}_{ALM}$ ) for the first two dominant spectral peaks across the tested  $\varepsilon/c$  values. The linear theory approximation maintains consistent accuracy, even with significant variations in  $C_l$  and  $\alpha_{eff,g}$  within a single period. This confirms the capability of the linear theory proposed in [12] to model unsteady aerodynamic flows beyond quasi-steady conditions.

The parameter  $\varepsilon/c$  plays a critical role in ALM simulations by controlling the spatial distribution of the body force and, consequently, the induced velocity at the actuator line in unsteady simulation [12]. Figure 11 illustrates the influence of  $\varepsilon/c$  on the effective angle of attack from ALM simulations ( $\alpha_{eff,ALM}$ ), computed using Equation 10. A smaller  $\varepsilon/c$  concentrates the body force near the actuator line, resulting

Table 1: Ratio of the induced velocity spectrum magnitude from ALM simulations and the linear theory

arepsilon/c	0.4	0.8	1.6
$\omega_{\hat{v}}/\Omega = 1$ $\omega_{\hat{v}}/\Omega = 2$	0.9899	1.0353	1.070
	1.0009	1.1146	1.1269

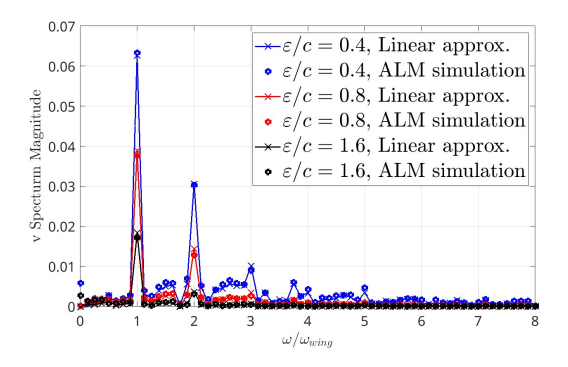


Figure 10: Induced velocity spectrum with different  $\varepsilon/c$ 

in a stronger normal induced velocity  $(u_y)$  and larger fluctuations in  $\alpha_{eff}$ . In contrast, a larger  $\varepsilon/c$  spreads the force more broadly, reducing the induced velocity and causing  $\alpha_{eff,ALM}$  to approach the geometric effective angle of attack  $\alpha_{eff,g}$ . This analysis shows that  $\varepsilon/c$  can significantly influence the effective angle of attack, even when aerodynamic forces from DNS are imposed.

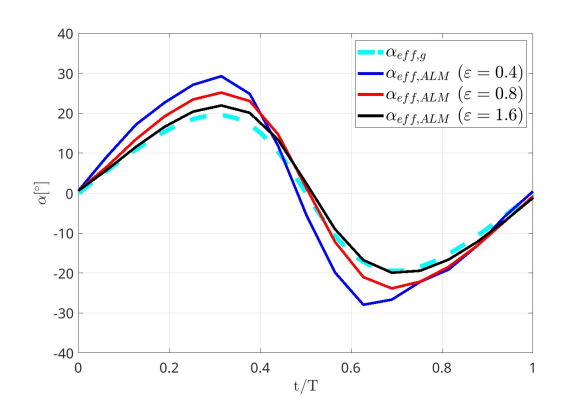


Figure 11: Effective angle of attack comparison with  $\varepsilon/c$ 

To further investigate the effective angle of attack derived from the linear theory and the influence of unsteady modifications in ALM, results for  $\varepsilon/c$  are compared. Figure 12 shows that incorporating the modification based on the pitching rate ( $\alpha_{eff,g}$ , see Equation 11) has a phase-shift effect on  $\alpha_{eff,ALM}$  in this case. Previous studies [12] indicate that  $\alpha_{eff,g}$  has a negligible impact for wings undergoing plunging motion at low reduced frequencies. However, the present results shows that the modification with pitching rate is not negligible for such a case with pitching motion, higher reduced frequency, and additional curvature effects, where dynamic stall is present. Moreover, the effective angle of attack predicted by the linear theory closely matches that from ALM

simulations. Combined with the spectral comparison in Figure 10, this confirms that the linear theory approximation captures key unsteady aerodynamic features, matching the force-imposed ALM results even at high lift and drag coefficients, where linear models often struggle.

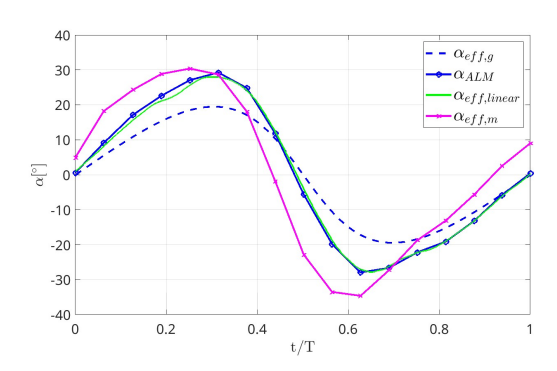


Figure 12: Different types of effective angle of attack comparison at  $\varepsilon = 0.4$ 

### 5 Conclusion

This study investigates the unsteady flow field around a wing traveling along a circular trajectory, focusing on the dynamic stall phenomenon. Direct numerical simulation (DNS) captures the evolution of the flow field, including the onset and development of the dynamic stall vortex, the trailing edge vortex roll-up, and their subsequent detachment from the wing surface. These flow features lead to significant variations in lift and pitching moment, highlighting the aeroelastic implications of dynamic stall. Proper orthogonal decomposition (POD) analysis provides insight into the dominant threedimensional vortical structures around the wing, revealing different stages of the dynamic stall process and contributing to a more comprehensive understanding of the unsteady aerodynamics involved. To evaluate actuator line method (ALM) capabilities, ALM simulations were conducted using aerodynamic forces imposed from DNS. The results demonstrate that the Gaussian width parameter  $\varepsilon/c$  plays a crucial role in determining the effective angle of attack, even when using high-fidelity force inputs. A smaller  $\varepsilon/c$  leads to stronger induced velocities and larger fluctuations in  $\alpha_{eff}$ , while a larger value results in a smoother response closer to the geometric angle of attack. Furthermore, a novel linear theory approximation for ALM was performed for unsteady flow conditions with high values of lift and drag. The theory shows good agreement with ALM simulation results, confirming its validity for modeling unsteady aerodynamic flows, including those involving dynamic stall. The proposed modification to account for the pitching rate was found to have considerable influence under high reduced-frequency conditions with significant variation of lift and drag. The finding from the present study advances the understanding of dynamic stall for wings following curved trajectories. It also demonstrates  $\varepsilon/c$  is an important parameter when using ALM in unsteady simulations. Therefore, this parameter should be carefully chosen to avoid errors introduced by the method. Moreover, it was shown that the linear theory can be employed to guide this choice, even for high values of forces typical of dynamic stall phenomena. With the current results underscoring the potential for modeling dynamic stall and unsteady aerodynamic effects with the actuator line method, further investigation with the incorporation of dynamic stall models to ALM, such as modification by Øye [24, 25] and other models, will facilitate the understanding the far wake behaviour of the unsteady aerodynamic flows with dynamic stall.

# Acknowledgement

The computation was performed on the high performance computing (HPC) cluster Dardel at PDC, KTH. The computations, data handling, and post-processing were enabled by resources provided by the National Academic Infrastructure for Supercomputing in Sweden (NAISS), partially funded by the Swedish Research Council through grant agreement no. 2022-06725.

### References

- [1] Daniel J. Garmann and Miguel R. Visbal. Control of dynamic stall on swept finite wings. *AIAA Journal*, (9), 2022.
- [2] Sébastien Le Fouest and Karen Mulleners. The dynamic stall dilemma for vertical-axis wind turbines. *Renewable Energy*, 2022.
- [3] Michael H. Dickinson, Fritz-Olaf Lehmann, and Sanjay P. Sane. Wing rotation and the aerodynamic basis of insect flight. *Science*, 1999.
- [4] Diana D. Chin and David Lentink. Flapping wing aerodynamics: from insects to vertebrates. *Journal of Experimental Biology*, 2016.
- [5] Prabal S. Negi, Recardo Vinuesa, Ardeshir Hanifi, Philipp Schlatter, and Dan S. Henningson. Unsteady aerodynamic effects in small-amplitude pitch oscillations of an airfoil. *International Journal of Heat and Fluid Flow*, 2018.
- [6] Miguel R. Visbal. Numerical investigation of deep dynamic stall of a plunging airfoil. *AIAA Journal*, (10), 2011.
- [7] Onur Son, An-Kang Gao, Ismet Gursul, Chris D. Cantwell, Zhijin Wang, and Spencer J Sherwin. Leading-edge vortex dynamics on plunging airfoils and wings. *Journal of Fluid Mechanics*, 2022.
- [8] Hsieh-Chen Tsai and Tim Colonius. Coriolis effect on dynamic stall in a vertical axis wind turbine. *AIAA Journal*, (1), 2011.
- [9] Jens N. Sørensen and Weng Zhong Shen. Numerical modeling of wing turbine wakes. *Journal of Fluid En*gineering, 2002.
- [10] Vitor G. Kleine, Ardeshir Hanifi, and Dan S. Henningson. Non-iterative vortex-based smearing correction for

- the actuator line method. *Journal of Fluid Mechanics*, 2023.
- [11] Vitor G. Kleine, Ardeshir Hanifi, and Dan S. Henningson. Simulating airplane aerodynamics with body forces: Actuator line method for nonplanar wings. *AIAA Journal*, (5), 2023.
- [12] Elías Alva, Vitor G. Kleine, and André V. G. Cavalieri. On the applicability of the actuator line method for unsteady aerodynamics. *arXiv preprint arXiv:2501.17395*, 2025.
- [13] Sébastien Le Fouest, Daniel Fernex, and Karen Mulleners. Time scales of dynamic stall development on a vertical-axis wind turbine blade. *Flow*, (E11), 2023.
- [14] Mukul Dave and Jennifer A. Franck. Analysis of dynamic stall development on a cross-flow turine blade. *Physical Review Fluids*, 2023.
- [15] Sangwoo Ahnn and Haecheon Choi. Leading-edge vortex and aerodynamic performance sacling in a simplified vertical-axis wind turbine. *Physics of Fluids*, 2023.
- [16] Brian Hand, Ger Kelly, and Andrew Cashman. Numerical simulation of a vertical axis wind turbine airfoil experiencing dynamic stall at high reynolds numbers. *Computers and Fluids*, 2017.
- [17] Yu-Cheng Lu, Ardeshir Hanifi, and Dan S Henningson. Numerical simulation of dynamic stall on vertical-axis wind turbine. *Journal of Physcis: Conference Series*, (012029), May 2025.
- [18] Paul F. Fischer, James W. Lottes, and Stefan G. Kerkemeier. Nek5000 website. https://nek5000.msc.anl.gov/, 2008. [Online; accessed 2025-06-06].
- [19] Brandon E. Merrill, Yulia T. Peet, Paul F. Fischer, and James W. Lottes. A spectrally accurate method for overlapping grid solution of incompressible navier–stokes equations. *Journal of Computational Physics*, 2016.
- [20] Suchuan S. Dong, George E. Karniadakis, and Chrysssostomos Chryssostomidis. A robust and accurate outflow boundary condition for incompressible flow simulations on severely-truncated unbounded domains. *Journal of Computational Physics*, 2014.
- [21] Robin B. Langtry and Florian R. Menter. Correlation-based transition modeling for unstructured parallelized computational fluid dynamics codes. *AIAA Journal*, (12), 2009.
- [22] Gal Berkooz, Philip Holmes, and John L. Lumley. The proper orthogonal decomposition in the analysis of turbulent flows. *Annual Review of Fluid Mechanics*, 1993.
- [23] Keaton J. Burns, Geoffrey M. Vasil, Jeffery S. Oishi, Daniel Lecoanet, and Benjamin P. Brown. Dedalus: A flexible framework for numerical simulations with spectral methods. *Physical Review Research*, 2(2), April 2020.

- [24] Stig Øye. Dynamic stall simulated as time lag of separation. In *Proceedings of the 4th IEA Symposium on the Aerodynamics of Wind Turbines*, volume 27, page 28. Rome, Italy, 1991.
- [25] M.H. Hansen, Mac Gaunaa, and Helge Aagaard Madsen. A Beddoes-Leishman type dynamic stall model in state-space and indicial formulations. Number 1354(EN) in Denmark. Forskningscenter Risoe. Risoe-R. 2004.